CHAPTER IV

VERTICAL TWO-PHASE FLOW REGIMES AND PRESSURE GRADIENTS: EFFECT OF VISCOSITY

4.1 ABSTRACT

The effect of liquid viscosity on the flow regimes and the corresponding pressure gradients along the vertical flow was investigated. Experiment was carried out in a vertical transparent tube of 0.019 m in diameter and 3 m in length and the pressure gradients were measured by the pressure taps connected to a U-tube manometer. Water and a 50 vol% glycerol solution were used as the working fluids whose kinematic viscosities were 0.85×10^{-6} and 4.0×10^{-6} m^2/s, respectively. In our air-liquid annular two-phase flow, the liquid film of various thicknesses flowed adjacent to the wall and the gas phase flowed at the center of the tube. The superficial air velocity, j_{air}, was varied between 0.0021 and 58.7 m/s and the superficial liquid velocity, j_{liquid}, was varied between 0 and 0.1053 m/s. In the bubble, the slug and the slug-churn flow regimes, as the Reynolds number of air increased the pressure gradients decreased. But in the annular and the mist flow regimes, pressure gradients increased with increasing Reynolds number.. Finally, the experimentally measured pressure gradient values were compared with the theoretical values and they were in good agreement.

(Key-words: vertical upward flow, liquid viscosity, pressure gradient, superficial gas /water velocity and Reynolds number)

Corresponding author: email anuvat.s@chula.ac.th, Ph: 662 218 4131, Fax: 662 611 7221

Corresponding author: email kitipat.s@chula.ac.th Ph: 662 218 4136, Fax: 662 215 4459

4.2 INTRODUCTION

Heat, mass and momentum transfer characteristics of two-phase flow depend strongly on its flow pattern. For the upward co-current two-phase flow, we can divide it into five flow regimes [1]: (1) bubble flow; (2) slug flow; (3) churn flow; (4) annular flow; and (5) mist flow. These regimes are important because of their influence on heat and mass transfer phenomena. This paper shall report an investigation of the flow patterns, the regimes, and the corresponding pressure gradients from the bubble flow to the annular mist flow.

Bubble flow is characterized by bubbles, which are small compared to the tube diameter. These bubbles are dispersed more or less randomly in the liquid continuum within the tube [2]. The bubble-to-slug transition is due to the collision between small bubbles, with a fraction of these collisions resulting in coalescence ultimately leading to bubbles which are of similar diameter to the pipe and hence to slug flow [3]. A bubble flow is only a transient flow regime, which, given a sufficiently long residence time in pipe, it will develop into a slug flow [3]. When a liquid flow is at a low rate, a highly disturbed flow with oscillatory nature can be formed corresponding to the intermediate regime between the annular and the slug flow regimes [4]. The distinctive flow pattern is called as a churn flow and the pressure gradient as well as the liquid holdup fluctuate violently [4].

The annular–mist flow regime is widely encountered in the flow of gas-liquid mixtures at high gas rates and gas-liquid ratios [5]. The annular flow regime in a gas-liquid system is characterized by an upward moving, continuous, smooth to wavy film of liquid on the tube wall and much more rapidly moving at the central core gas, containing entrained droplets of liquid in a concentration which may vary

from a low to a high concentration. The liquid film may be wholly in a laminar motion or it may be a laminar state only nearest the wall, and a turbulent state nearest the gas-liquid interface [5]. Annular flow is the most predominant flow pattern found in evaporators, natural gas pipelines, and steam heating systems [6]. With the further increase in the gas flow rate, the liquid film becomes progressively thinner while the number of the droplets in the core flow increases. Finally, the film will be removed from the wall and a pure mist flow occurs [6].

The objectives of this paper are to investigate the effect of liquid viscosity on the flow patterns, the flow regimes and the corresponding pressure gradients in each flow regime. The pressure gradient data from the experiment are compared with those predicted from the theory proposed in the literature.

4.3 EXPERIMENTAL APPARATUS

The scheme of the experimental setup is shown in figure 1. Air and two different liquids, i.e., water and aqueous glycerol solution with different liquid viscosities, were used as the testing fluids. Their properties are tabulated in table 1. The main components of the system consisted of a vertical test section, an air supply, an aqueous glycerol solution supply tank and instrumentation. The test section, with an inside diameter of 0.019 m and the length of 3 m was made of a transparent acrylic glass to permit visual observation of the flow patterns. The hydrodynamics of the two-phase flow from the bubble to the annular and the mist flows were studied in the main column. Compressed air from the compressor [Taiwan, Fu Sheng HTA-100] with constant 1 bar entered at the bottom of the main column and flow rates were measured by a calibrated air-rotameter [Cole-Parmer, U.S.A, A-32466-68].

Water or aqueous glycerol solution was pumped from the storage tank through the liquid-rotameter and mixed with air at the bottom of the main column. The flow rates of water or aqueous glycerol solution were also measured by a liquid-rotameter [Cole-Parmer, U.S.A, A-32461-42]. The liquid from the main column flowed upward together with air and then flowed back into the storage tank. Two static pressure tabs were installed at two axially locations with the spacing of 0.4 m and connected with a custom made manometer which was used to measure the pressure drops along the test section.

The experimental conditions were as follows: superficial air velocity j_{air}: 0.0021~58.7 m/s, superficial water velocity j_{water}: 0.0131~0.0703 m/s, and superficial aqueous glycerol solution velocity $j_{solution}$: 0.0121~ 0.1053 m/s, respectively. The pressure at the exit of the tube was about 100 kPa and air and liquid temperatures varied between 31~32°C. The aqueous glycerol solution's viscosity was measured before and after the experiments and it was found to be nearly the same to within few percents. Before taking any data from the experiment, the system was allowed to be in a steady state condition. The pressure drops across the test section were detected at different flow rates of air and liquid. The flow regimes were observed and identified by visual observation, still photographs [Nikon, Japan, D 100] and a video camera [Sony, Japan, 700×Digital].

4.4 RESULTS AND DISCUSSION

4.4.1 Visual observations of the flow by still photographs

Figure 2 shows the still photographs of the different flow regimes from the two-phase flow experiment. When the superficial liquid velocity, j_{liquid}, and

the superficial air velocity, j_{air} were low, bubble flow can be seen as shown in figure 2 (a). The flow pattern basically changed from bubble flow to mist flow with increasing j_G at a fixed j_L value. As the superficial air velocity, j_{air}, was increased, the flow regime changed to slug, churn, annular, and mist flow regimes respectively. Figures 2 (a) to 2 (e) show various flow regimes for air-water mixture and figures 2 (f) to 2 (j) show the corresponding flow regimes for air-50 vol% glycerol solution mixture.

4.4.2 Flow pattern maps for pure water and 50 vol% glycerol solution

Figure 3 (a) shows the flow pattern regimes of air-water and air-50 vol% glycerol mixture, respectively for our two-phase vertical flows. Thin solid lines represent the critical Reynolds number of air, $(Re_{air})_{critical}$ for each flow regime and identify the boundaries of the flow patterns observed. All the boundaries between bubble-slug, slug, slug-churn, churn, annular, and mist regimes were identified by direct visual observation of the flow patterns as well as by observations through the digital camera and the video. Figure 3 (b) shows the flow pattern regimes for the air-50 vol% glycerol solution in two-phase flow. The viscosity of the liquid affected the boundaries of the flow patterns in the bubble, the bubble-slug, and the slug flow regimes. In these flow regimes, the Reynolds numbers of air for each regime, $(Re_{air})_{critical}$ were lower than 2000 and the flow was presumably laminar. [Wilkes, 1999]. The boundaries of the bubble flow , the bubble-slug, and the slug flow regimes shifted to the right relative to those of figure 3(a) because of the increase in viscosity at about same Reynolds number of each liquid ,$Re_{water} = 0$, $Re_{solution} = 0$;

Re_{water} = 293, $Re_{solution}$ = 307; Re_{water} = 427, $Re_{solution}$ = 435; and Re_{water} = 560, $Re_{solution}$ = 500.

Therefore, the critical Reynolds number of air, $(Re_{air})_{critical}$ or the boundaries of the flow pattern lines moved right in the bubble, the bubble–slug transition, and the slug flow regimes due to the difference in viscosity even under the same Re_{air} and Re_{liquid} conditions. When we increased the liquid viscosity from 0.85224×10^{-6} m^2/s to 4.0×10^{-6} m^2/s, the bubbles forming in the bubble flow regime were lesser in number at low Re_{air} because of the viscosity effect. Therefore, the bubble collisions between small bubbles resulting in coalescence were also less and the gradual coalescence process leading to the bubble-slug transition was more extended than that of pure water. In summary, the boundary lines of those flow regimes moved to the right in comparison with those of the air-pure water system. For the churn, the annular, and the mist flow regimes, air Reynolds numbers, Re_{air} were high and the flow is highly turbulent, and the viscosity effect on the boundaries was less. Therefore, in these flow regimes, the effect of viscosity was not pronounced and the boundaries remained mostly the same.

4.4.3 Pressure gradients for pure water and 50 vol% glycerol solution

Figure 4 shows the variation of the measured pressure gradients, $(-dp/dz)_{exp}$, with air Reynolds numbers, Re_{air}. In figures 4 (a) to 4 (f), we compare the pressure gradients of the pure water and 50 vol% glycerol solutions at the same liquid Reynolds numbers. The pressure gradients decreased steadily with increasing Re_{air} from the bubble to the slug-churn flows for both the pure water and aqueous glycerol solutions. But in the churn flow, the pressure gradients increased slightly

and decreased again. Finally, we enter the annular flow regime where the pressure gradients, $(-dp/dz)_{exp}$, increased with increasing air Reynolds numbers. At the same liquid Reynolds numbers, the pressure gradients, $(-dp/dz)_{exp}$, of the higher viscosity aqueous glycerol solution were always higher than the pressure gradients, $(-dp/dz)_{exp}$, of the pure water.

In figure 4 (a), the flow rates for the pure water and aqueous glycerol solution were zero; therefore we could only obtain data up to the slug flow regime. From figures 4 (b) to 4 (f), we present the measured pressure gradients from the bubble to the mist flow regimes. Fluctuations in the pressure gradients, $(-dp/dz)_{exp}$, occurred in the bubble to the churn flow regimes but they were more stable in the bubble, the annular and the mist flow regimes. Fluctuations of pressure gradients, $(-dp/dz)_{exp}$, were less in the aqueous glycerol solution than those in the pure water. This was probably the effect of viscosity on the pressure gradients in our system. At low water Reynolds numbers, the pressure gradients were more stable in the bubble and the bubble-slug transition flow regimes. When we increased the Reynolds number of water apparently then fluctuations started to occur in the bubble and the bubble-slug transition flow regimes. But in the aqueous glycerol solution, increasing the liquid Reynolds numbers did not affect significantly the pressure gradient fluctuations in all regimes. The highest fluctuations occurred in the slug and the slug-churn transition for both the pure water and aqueous glycerol solutions.

4.4.4 Comparison between theoretical and measured pressure gradients, (-dp/dz)

Figure 5 shows the comparison between the predicted $(-dp/dz)_{cal}$ from the theory [6,10], $(-dp/dz)_{cal}$, and the measured values $(-dp/dz)_{exp}$, as obtained from experiments. From figures 5 (a) to 5 (i), we compared the predicted values and the measured values in the bubble, the slug, the annular and the mist flow regimes. The pressure gradients encountered in the two-phase flow system is one of the most important parameters in understanding the behavior of the system.

4.4.4.1 Bubble flow regime

The predicted pressure gradients, $(-dp/dz)_{cal}$ for bubble flow regime are proposed by Nicklin, Wilkes, and Davidson [7] as in the following equation:

$$\left(-\frac{dp}{dz}\right) = \rho_L \, g \, (1-\varepsilon) \tag{1}$$

where ρ_L = liquid density (kg/m^3), g = gravitational acceleration constant (m/s^2), and ε = void fraction of air. This equation implies that the predicted $(-dp/dz)_{cal}$ can be determined if the liquid density, ρ_L, and void fraction of air, ε, were known. The void fraction of air, ε, was also proposed by Nicklin, Wilkes, and Davidson [7] from the following equation if Q_G and Q_L are known.

$$\text{Void fraction} = \varepsilon = \frac{Q_G}{(Q_G + Q_L) + u_b \, A} \tag{2}$$

where Q_G = volumetric flow rate of gas (l/min), Q_L = volumetric flow rate of liquid (l/min), A = cross-sectional area of the pipe (m^2), (-dp/dz) = pressure gradient (kPa/m), u_b = bubble rise velocity in a stagnant liquid (m/s). The bubble velocity, u_b rising into a stagnant liquid was proposed by Peebles and Garber [10].

$$\text{Bubble velocity} = u_b = 1.00\sqrt{g\,R_b} \tag{3}$$

where g = gravitational acceleration constant (m/s^2), R_b = radius of the bubble (m).

Figure 6 shows the diameters of the different bubble sizes. Bubbles diameters can be measured from the still photos and the diameters were from 0.014~0.0145 m for the air–pure water mixture and 0.0145~0.0152 m for the air-50 vol% glycerol solution mixture.

4.4.4.2 Slug flow regime

The predicted pressure gradient,$(-dp/dz)_{cal}$ for the slug flow regimes was proposed by Nicklin, Wilkes, and Davidson as in the following equation [7]:

$$\left(-\frac{dp}{dz}\right) = (1-\varepsilon)\left[\rho_L\, g + \left(\frac{dp}{dz}\right)_{sp}\right] \tag{4}$$

Single-phase frictional pressure gradient for the liquid only is:

$$\left(-\frac{dp}{dz}\right)_{sp} = \frac{2 f_F\, \rho_L \overline{u_L}^2}{D} \tag{5}$$

The single-phase pressure gradients were calculated with the friction factors, $f_F = 16/\mathrm{Re}$ for laminar flow (Re < 2000), and $f_F = 0.0790\,\mathrm{Re}^{-1/4}$ for turbulent flow (Re > 4000). The Reynolds number of the liquid, $\mathrm{Re}_L = \left(\overline{u_L}\, D\right)/\nu_l$ and mean upward liquid velocity, $\overline{u_L}$ can be calculated from, $\overline{u_l} = (Q_G + Q_L)/A$. The calculation of the void fraction of air, ε, was proposed from the following equation by Nicklin, Wilkes, and Davidson [7]:

$$\text{Void fraction} = \varepsilon = \frac{Q_G}{1.2(Q_G + Q_L) + u_b\, A} \tag{6}$$

where Q_G = volumetric flow rate of gas (l/min), Q_L = volumetric flow rate of liquid (l/min), A = cross-sectional area of the pipe (m^2), u_b = bubble rise velocity in a stagnant liquid (m/s).

The bubble rise velocity, u_b rising into a stagnant liquid was proposed by Davies and Taylor [8] as in the the following equation:

$$\text{Bubble rise velocity} = u_b = c\sqrt{g\,D} \tag{7}$$

where g = gravitational acceleration constant (m/s^2), D = diameter of the pipe (m). The experiments indicate that the constant "c" was 0.35 [8].

4.4.4.3 Annular and mist flow regimes

The pressure gradients, $(-dp/dz)_{cal}$ for the annular and the mist flows were proposed by Wallis [6]; it uses the Lockhart-Martinelli correlation [9] for the friction part of the pressure gradient, and supplemented with appropriate gravitational terms. We now consider two parts for the pressure gradient calculation. First, consider just the flow of gas in the inner core. The momentum equation for the gas core was proposed by Wallis [6] as:

$$\left(\frac{dp}{dz}\right)_{tp} = \left(\frac{dp}{dz}\right)_{g} = -\frac{2 f_F\ \rho_g\ v_g^2}{D_g} - \rho_g g = \phi_g^2 \left(\frac{dp}{dz}\right)_{go} - \rho_g g \tag{8}$$

Second, the momentum equation for the entire flow was also proposed by Wallis (1969):

$$\left(\frac{dp}{dz}\right)_{tp} = \phi_l^2 \left(\frac{dp}{dz}\right)_{lo} - \left[\varepsilon\,\rho_g + (1-\varepsilon)\,\rho_l\right] g \tag{9}$$

Eliminating the two-phase pressure gradient between these two equations gives a single equation with three unknowns, ϕ_g^2 = the gas two-phase flow multiplier, ϕ_l^2 = the liquid two-phase flow multiplier, and ε = the void fraction of air. In the Lockhart-Martinelli model [9], the gas two-phase flow multiplier ϕ_g is defined as:

$$\phi_g^2 = \frac{(dp/dz)_{tp}}{(dp/dz)_{go}} \tag{10}$$

where $(dp/dz)_{tp}$ is two-phase pressure gradient, and $(dp/dz)_{go}$ is the gas only pressure gradient. The Lockhart-Martinelli model [9] provides correlations for the multiplier based on the Martinelli parameter defined as:

$$X^2 = \frac{(dp/dz))_{lo}}{(dp/dz)_{go}} = \frac{\phi_g^2}{\phi_l^2} \tag{11}$$

where $(dp/dz)_{lo}$ is the pressure gradient of the liquid flowing alone in the tube. The correlations between X, ϕ_g and ε *is:*

$$\phi_g = \left(1 + X^{2/n}\right)^{n/2} \tag{12}$$

$$\varepsilon = \frac{1}{\left(1 + 0.0904\, X^{0.548}\right)^{2.82}} \tag{13}$$

where the exponent for two-phase correlation "n" based on the gas/liquid phase laminar or turbulent flow [10]. Finally, we put these correlations into a single equation with three unknowns, ϕ_g^2, X, and ε and obtain the general equation to find "X" for pure water and 50 vol% glycerol solution. The Martinelli parameter "X" can be calculated from the single-phase pressure gradient using the standard friction factor approach. For pure water, "X" is defined as:

$$\left(1+X^{2/3.61}\right)^{3.61}\left((dp/dz)_{go}-\frac{(dp/dz)_{lo}}{X^2}\right)=9749\left(1-\frac{1}{\left(\left(1+0.0904X^{0.548}\right)^{2.82}\right)}\right) \quad (14)$$

We get this equation by equating the equation (8) and (9) and eliminating two-phase pressure gradient to get the single equation with three unknowns, ϕ_g^2, ϕ_l^2 and ε. And we replace ϕ_l^2 with Martinelli parameter "X" by using equation (11), replace ϕ_g^2 with Martinelli parameter "X" by using equation (12) and replace ε with equation (13) in order to get equation (14) for simply calculation.

For 50 vol% glycerol solution, the parameter "X" is defined as:

$$\left(1+X^{2/3.61}\right)^{3.61}\left((dp/dz)_{go}-\frac{(dp/dz)_{lo}}{X^2}\right)=10985.4\left(1-\frac{1}{\left(\left(1+0.0904X^{0.548}\right)^{2.82}\right)}\right) \quad (15)$$

When the value of X is determined, ϕ_g is calculated from equation (12). The two-phase pressure gradient, $(-dp/dz)_{tp}$ then can be calculated from equation (8).

We used the Lockhart-Martinelli model [9] to obtain the predicted pressure gradients, $(-dp/dz)_{cal}$ and compared them with the measured pressure gradients, $(dp/dz)_{exp}$ in annular and mist flows. The single-phase pressure gradients were calculated with friction factors, $f = 16/Re$ for $Re < 2000$ and $f = 0.0791 / (Re^{1/4})$ for $Re > 4000$.

Figure 5 (c) to 5 (i) shows the comparison between the measured $(-dp/dz)_{exp}$ and the predicted $(-dp/dz)_{cal}$ using equations (8) to (15). At low water Reynolds number, Re_{water}, the predicted $(-dp/dz)_{cal}$ values from the theory agree well with the measured $(-dp/dz)_{exp}$ values. At high water Reynolds number, the predicted $(-dp/dz)_{cal}$ values were lower than the measured values in the annular and the mist

flow regimes. For 50 vol% glycerol solution, the predicted $(-dp/dz)_{cal}$ values are always lower than the measured $(-dp/dz)_{exp}$ values.

Comparison of predicted values for the pressure gradients obtained from this prediction method, $(-dp/dz)_{cal}$, and the measured values $(-dp/dz)_{exp}$ are shown in figures 7 and 8. As can see in figure 7, the predicted values agreed with measured data within an accuracy of ± 10% for bubble flow, ± 15% for slug flow and ± 40% for annular and mist flows in air-pure water mixture.

In figure 8, the predicted values agreed with measured data within an accuracy of ± 15% for the bubble flow, ± 30% for the slug flow and ± 40% for the annular and the mist flows for the air-50 vol% glycerol solution mixture.

4.5 CONCLUSIONS

The experiments were carried out on the isothermal two-phase upward flows in a vertical tube with an inner diameter 0.019 m for air-water and air-50 vol% glycerol solution systems in order to observe and understand the effect of viscosity on the flow pattern regimes and the pressure gradient in each flow regime.

As the liquid viscosity increases, the boundaries of the bubble, the bubble-slug and the slug flow regimes in aqueous glycerol solution shifted to the right relative to those of pure water. But the boundaries for the churn, the annular and the mist flow regimes remained nearly the same. In the bubble, the bubble-slug and the slug flows, the critical Reynolds numbers of air, $(Re_{air})_{critical}$ were low and the flow was laminar. So, the effect of viscosity was more pronounced in these regimes. For the churn, the annular and the mist flows, the critical Reynolds numbers of air,

$(Re_{air})_{critical}$ were high and the flow was turbulent. So, The effect of viscosity in these regimes were relatively less.

Fluctuations of pressure gradients, $(-dp/dz)_{exp}$, were less in the aqueous glycerol solution than those in pure water because of the viscosity effect. The highest fluctuations occurred in the slug and the slug-churn transition regimes of both pure water and the aqueous glycerol solutions.

The proposed theories for the pressure gradient by Nicklin, Wilkes, and Davidson (1962) for the bubble and the slug flow regimes and by Wallis (1969) for the annular and the mist flow regimes are in moderately good agreement with measured values.

4.6 ACKNOWLEDGEMENTS

This work was supported by Postgraduate Education and Research Programs in Petroleum and Petrochemical Technology (PPT Consortium under ADB fund), and the Conductive and Electroactive Polymer Research Unit, Chulalongkorn University.

4.7 REFERENCES

[1] G.F. Hewitt, G.L. Shires, T.R. Bott, Process Heat Transfer, CRC Press, 1994, Chapter 10.

[2] H. Cheng, J.H. Hills, B.J. Azzorpardi, A study of the bubble-to-slug transition in vertical gas-liquid flow in columns of different diameter, International Journal of Multiphase flow 24 (3) (1998) 431-452.

[3] N.A. Radovich, R. Moissis, The transition from two-phase bubble flow to slug flow, MIT Report, Report No. 7-7673-22, (1962).

[4] T. Sawai, M. Kaji, T. Kasugai, H. Nakashima, T. Mori, Gas-liquid interfacial structure and pressure drop characteristics of churn flow, Experimental Thermal and Fluid Science 28 (3) (2003) 597-606.

[5] G.W. Govier, K. Aziz, The Flow of Complex Mixtures in Pipes, Van Nostrand Reinhold, New York, 1972.

[6] G.B. Walllis, One-dimensional Two-phase Flow, McGraw Hill, New York, 1969.

[7] D.J. Nicklins, J.O. Wilkes, J.F. Davidson, Two-phase flow in vertical tubes, Transactions of the Institute of Chemical Engineer 40 (3) (1962) 61-68.

[8] R.M. Davies, G.I. Taylor, The mechanics of large bubbles rising through extended liquids and through Liquids in tubes, Proceedings of the Royal Society, 200A, (1950) 375-390.

[9] R.W. Lockhart, R.C. Martinelli, Proposed correlation of data for isothermal two-phase, two-component flow in pipes, Chemical Engineering Progress 45 (1) (1949) 39-48.

[10] J.O. Wilkes, Fluid Mechanics for Chemical Engineers, Prentice-Hall PTR, New Jersey, 1999.

[11] S. Wongwises, W. Kongkiatwannitch, Interfacial friction factor in vertical upward gas-liquid annular two-phase flow, International Communications in Heat and Mass Transfer 28 (3) (2001) 323-336.

[12] T. Fukano, T. Furukawa, Prediction of the effects of liquid viscosity on interfacial shear stress and frictional pressure drop in vertical upward gas-liquid annular flow, International Journal of Multiphase Flow 24 (4) (1998) 587-603.

Table 4.1 Physical properties of liquids used in the experiment (2.Experimental Apparatus)

Liquid	ν_L (m^2/s)	ρ_L (kg/m^3)	μ (kg/m.s)
Water	0.85×10^{-6}	995	8.48×10^{-4}
50 vol% glycerol solution	4.0×10^{-6}	1121	4.48×10^{-3}

Note:

ν_L: kinematic viscosity, ρ_L: density, μ: viscosity

System temperature, T = 31°C (± 1°C)

System pressure, Pr = 1 bar

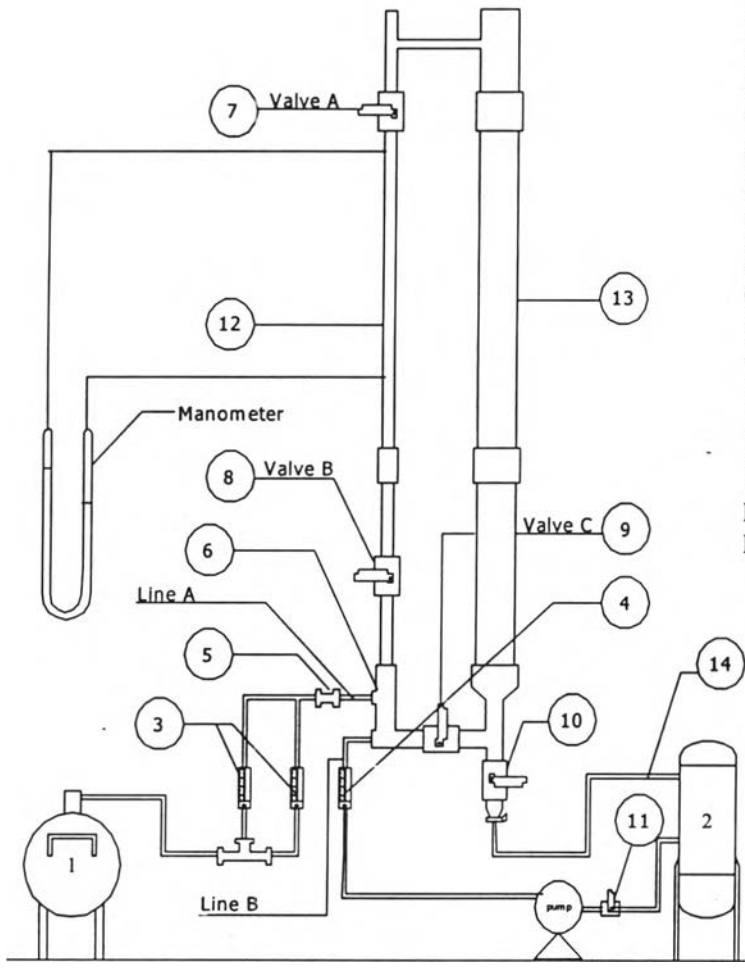

1. Air compressor maximum 10 bar
2. Solution reservoir tank
3. Air rotameter
4. liquid rotameter
5. check value
6. Air injection tee
7. Ball valve A
8. Ball valve B
9. Ball valve C
10. Draining ball valve
11. Control valve for reservoir tank
12. Acrylic tube (1.9 cm)
13. Overflow acrylic tube (5.4 cm)
14. Solution return line to reservoir

Line A Air injection line
Line B Solution injection line

Figure 4.1 Schematic diagram of the experimental setup (modified from Puengpatipan, 2002).

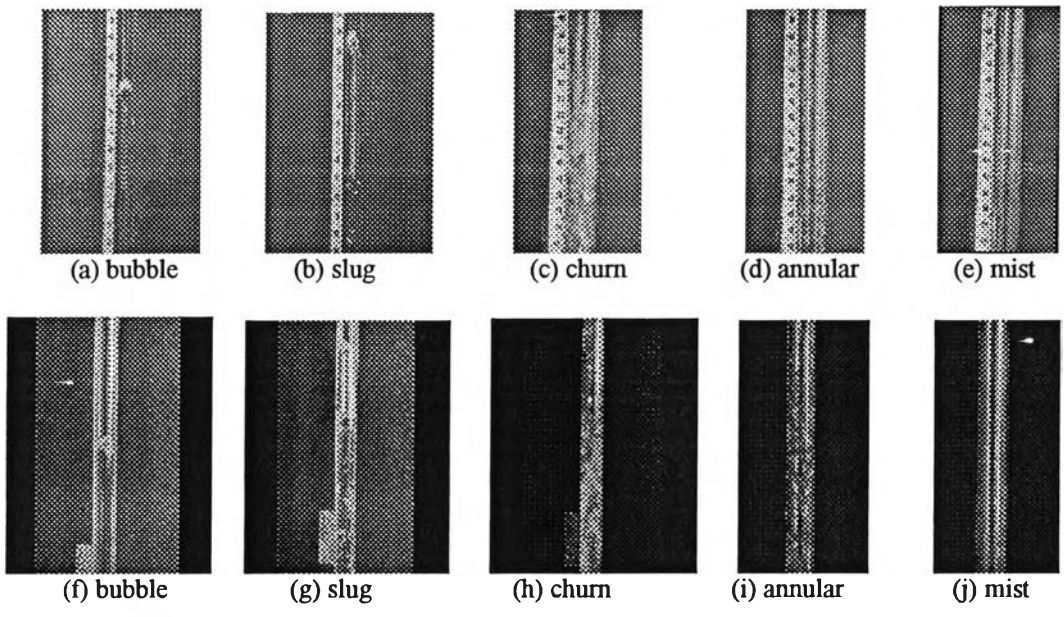

Figure 4.2 Different flow regimes for air-water mixture and air-50 vol% glycerol solution mixture:

a) j_{water} = 0.0131 m/s, Re_{water} = 293, j_{air} = 0.0042 m/s, Re_{air} = 5.05;

b) j_{water} = 0.0131 m/s, Re_{water} = 293, j_{air} = 0.0232 m/s, Re_{air} = 28.07;

c) j_{water} = 0.0131 m/s, Re_{water} = 293, j_{air} = 2.93 m/s, Re_{air} = 28.07 ;

d) j_{water} = 0.0131 m/s, Re_{water} = 293, j_{air} = 17.61 m/s, Re_{air} = 21319;

e) j_{water} = 0.0131 m/s, Re_{water} = 293, j_{air} = 46.95 m/s, Re_{air} = 56852;

f) $j_{solution}$ = 0.1053 m/s, $Re_{solution}$ = 500, j_{air} = 0.0115 m/s, Re_{air} = 13.95;

g) $j_{solution}$ = 0.1053 m/s, $Re_{solution}$ = 500, j_{air} = 0.141 m/s, Re_{air} = 170.93;

h) $j_{solution}$ = 0.1053 m/s, $Re_{solution}$ = 500, j_{air} = 2.35 m/s, Re_{air} = 2842;

i) $j_{solution}$ = 0.1053 m/s, $Re_{solution}$ = 500, j_{air} = 23.47 m/s, Re_{air} = 28426;

j) $j_{solution}$ = 0.1053 m/s, $Re_{solution}$ = 500, j_{air} = 46.95 m/s, Re_{air} = 56852.

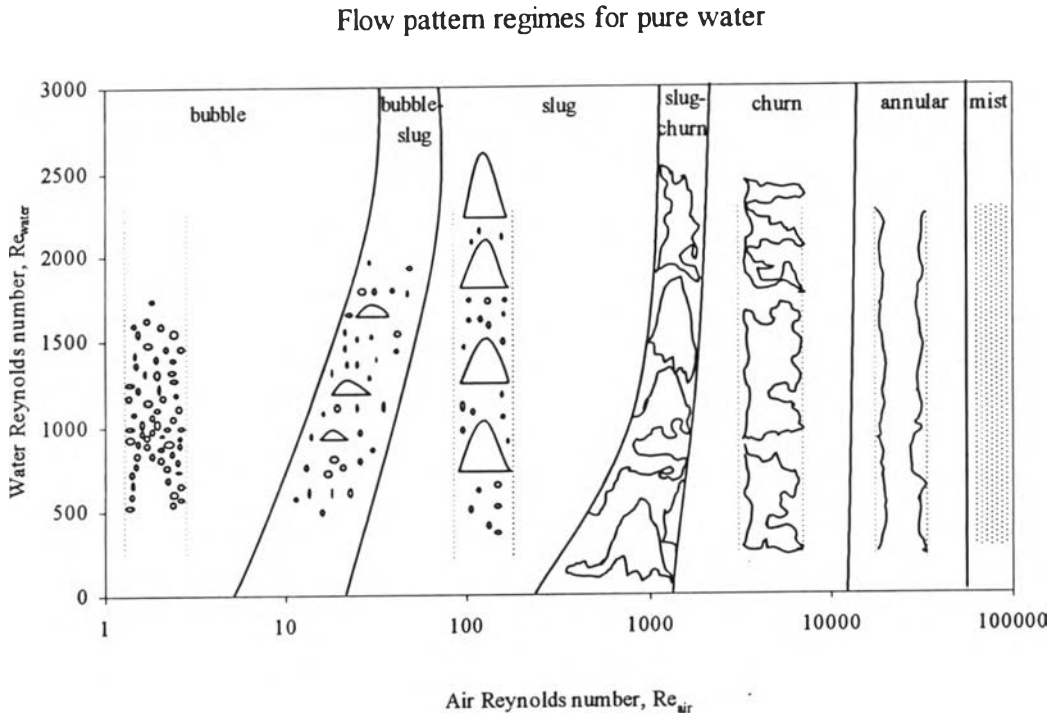

Figure 4.3 (a) Flow pattern regimes for air-pure water mixture.

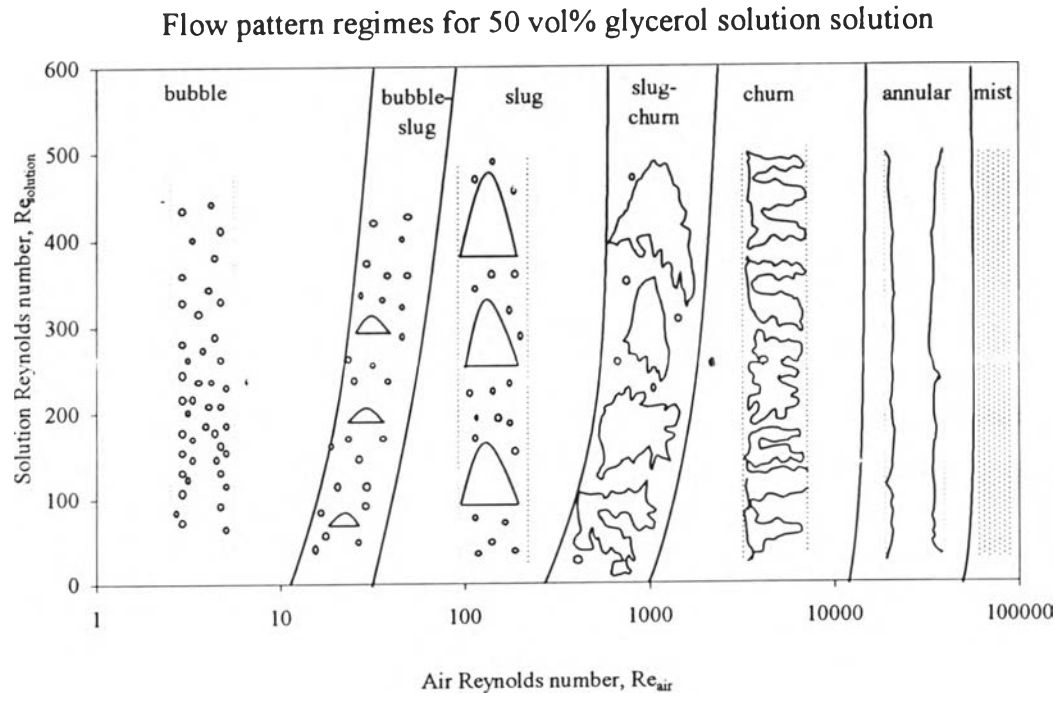

Figure 4.3 (b) Flow pattern regimes for air-50 vol% glycerol solution mixture.

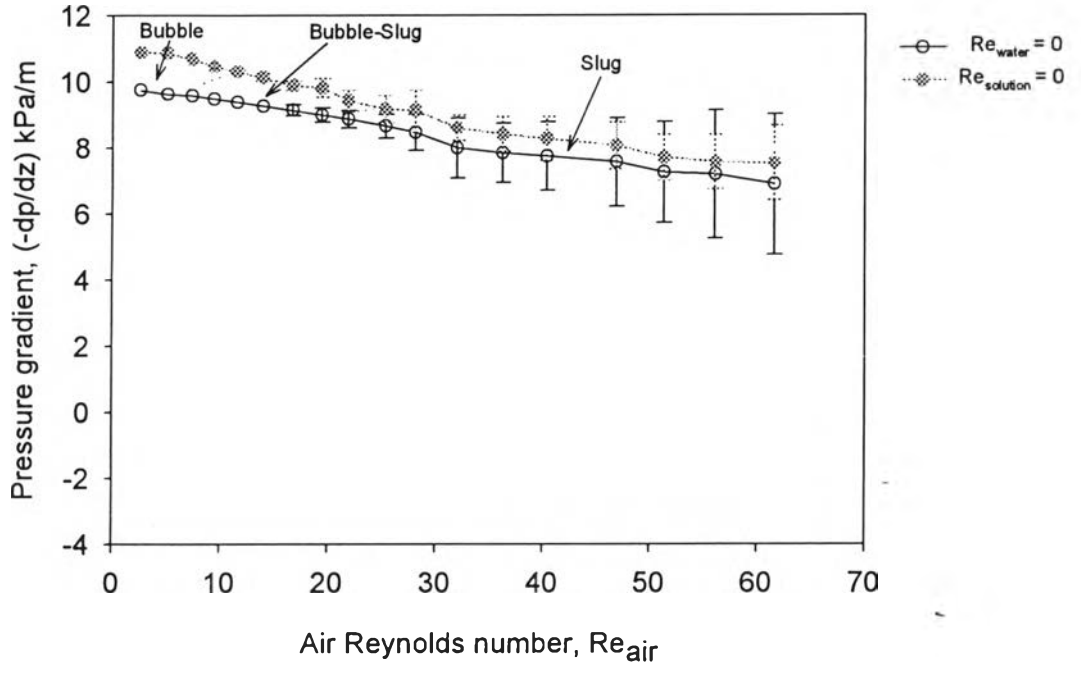

Figure 4.4 (a) Pressure gradient vs. air Reynolds number of pure water and 50 vol% glycerol solution.

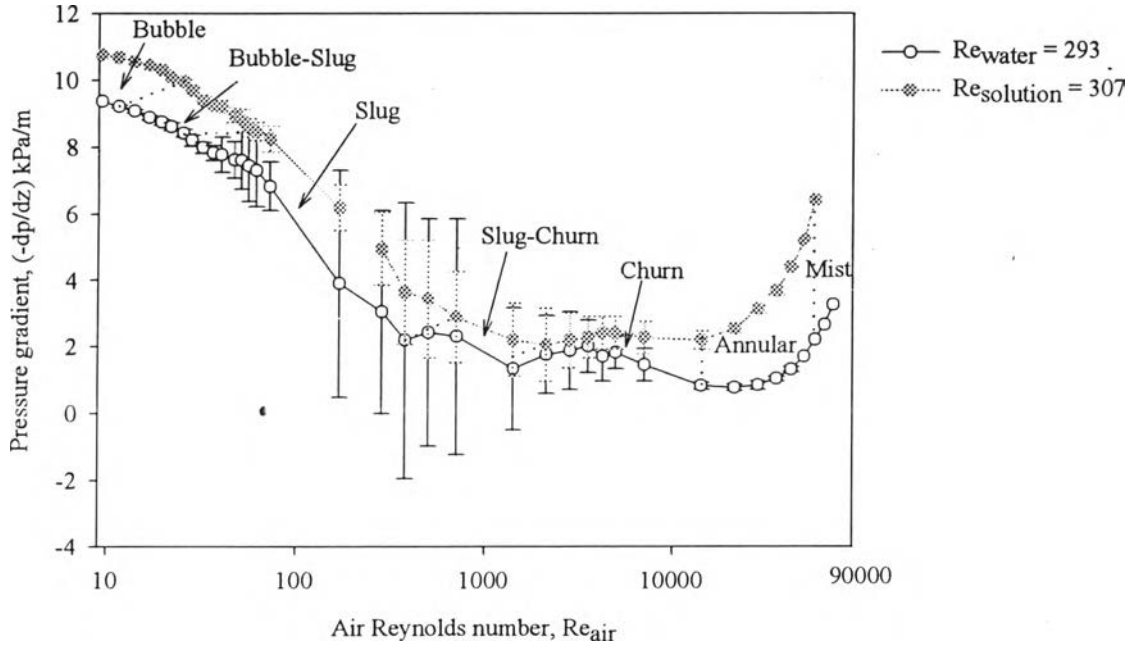

Figure 4.4 (b) Pressure gradient vs. air Reynolds number of pure water and 50 vol% glycerol solution.

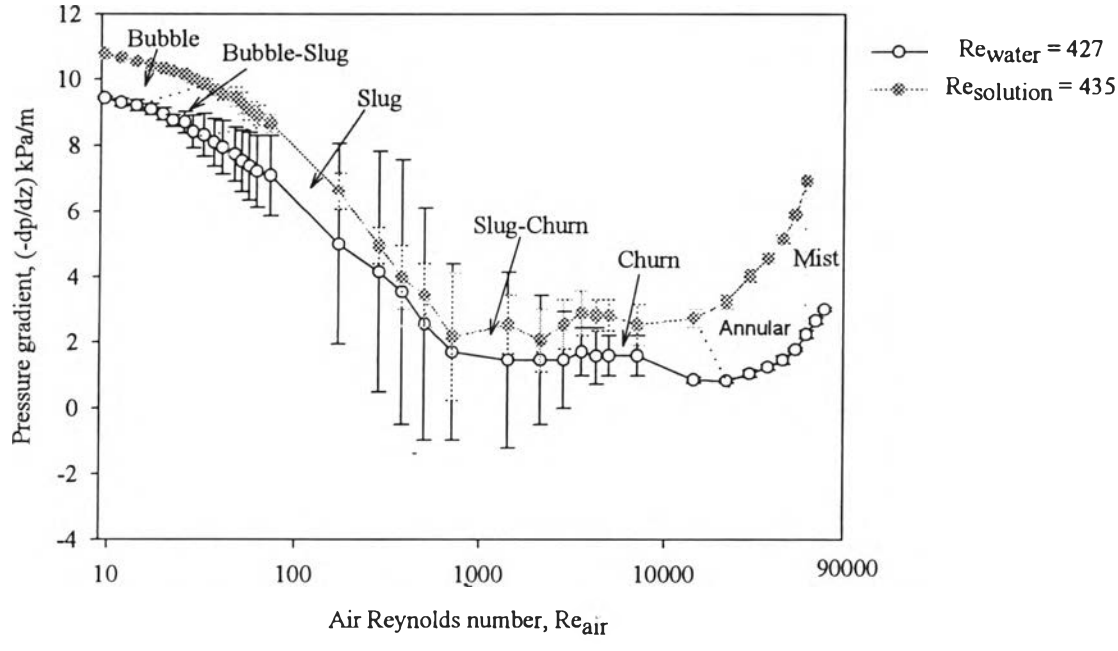

Figure 4.4 (c) Pressure gradient vs. air Reynolds number of pure water and 50 vol% glycerol solution

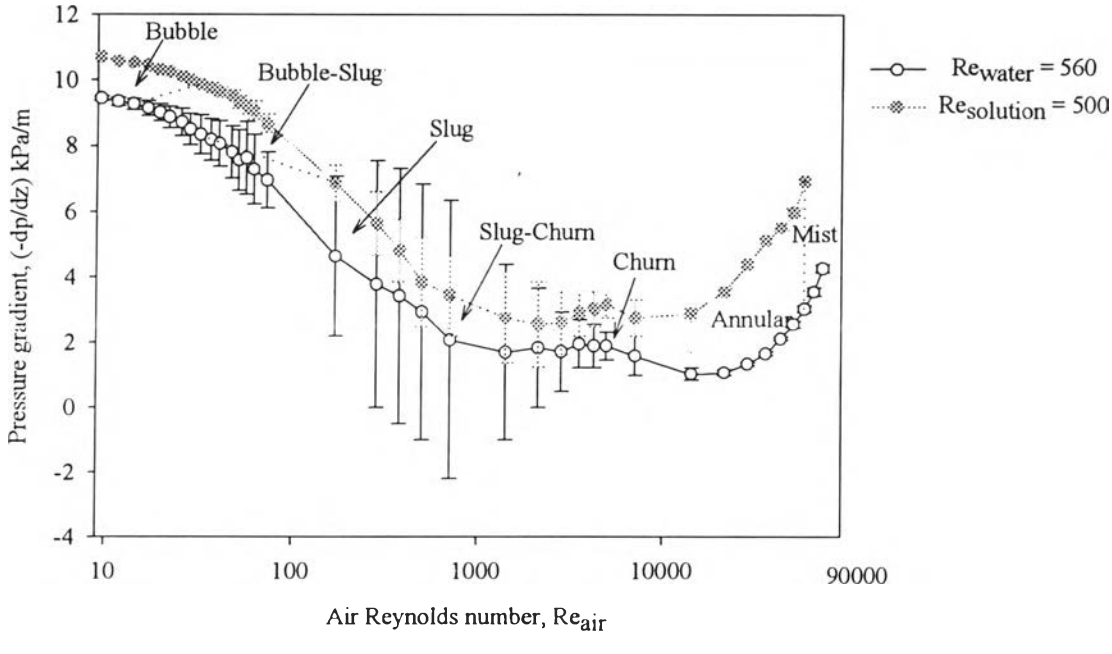

Figure 4.4 (d) Pressure gradient vs. air Reynolds number of pure water and 50 vol% glycerol solution.

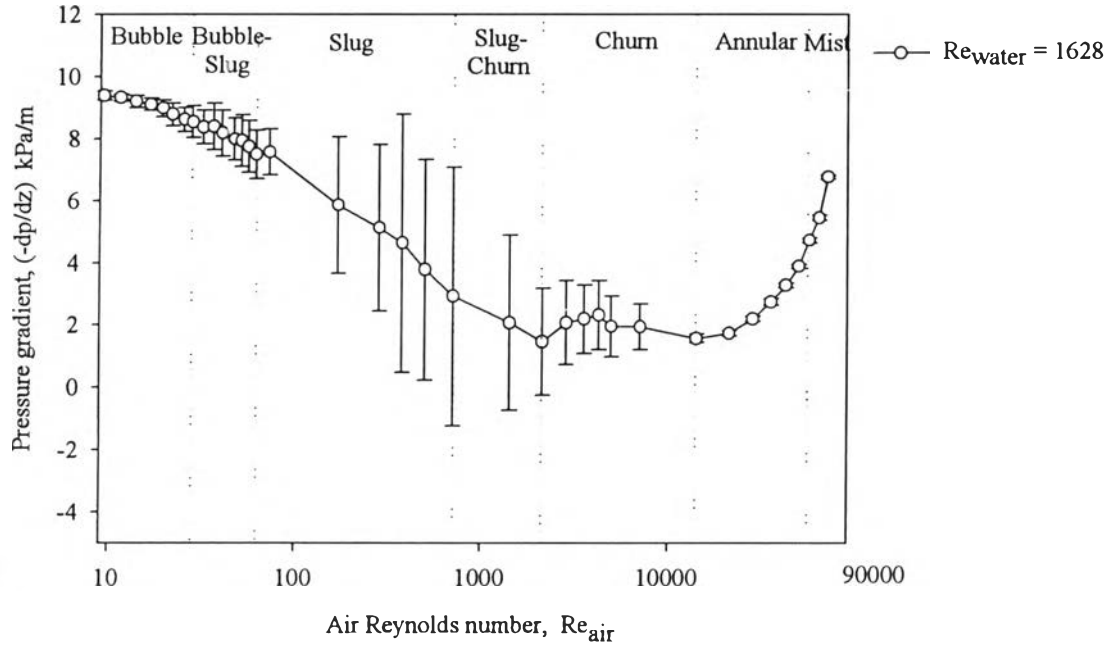

Figure 4.4 (e) Pressure gradient vs. air Reynolds number of pure water.

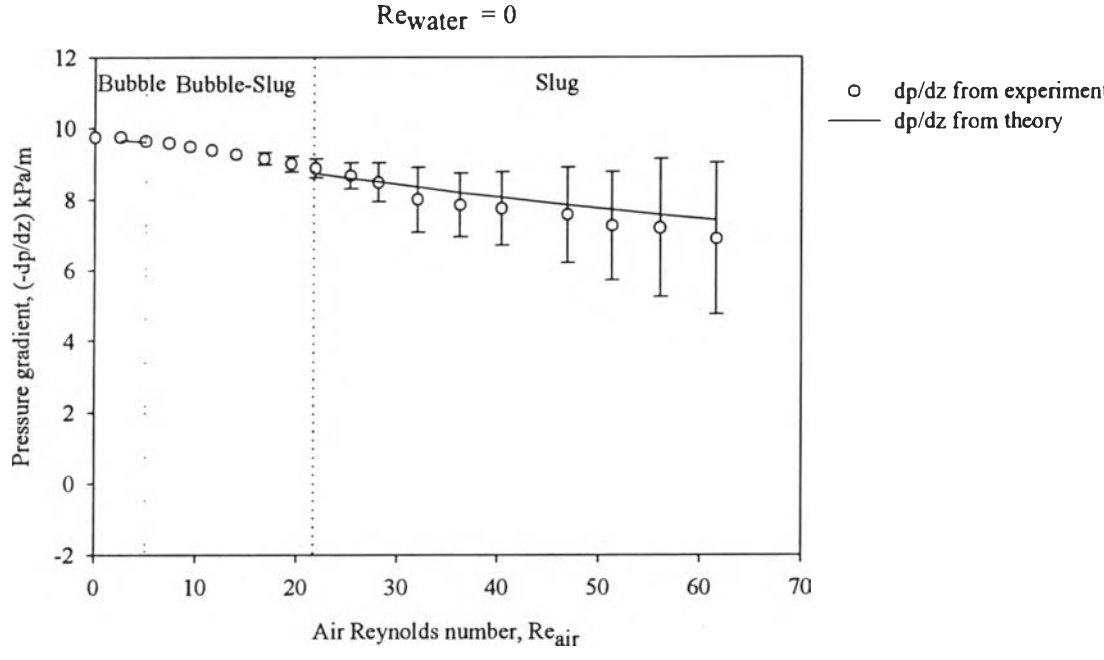

Figure 4.5 (a) Comparison between theory and experimental pressure gradient vs. air Reynolds number of pure water.

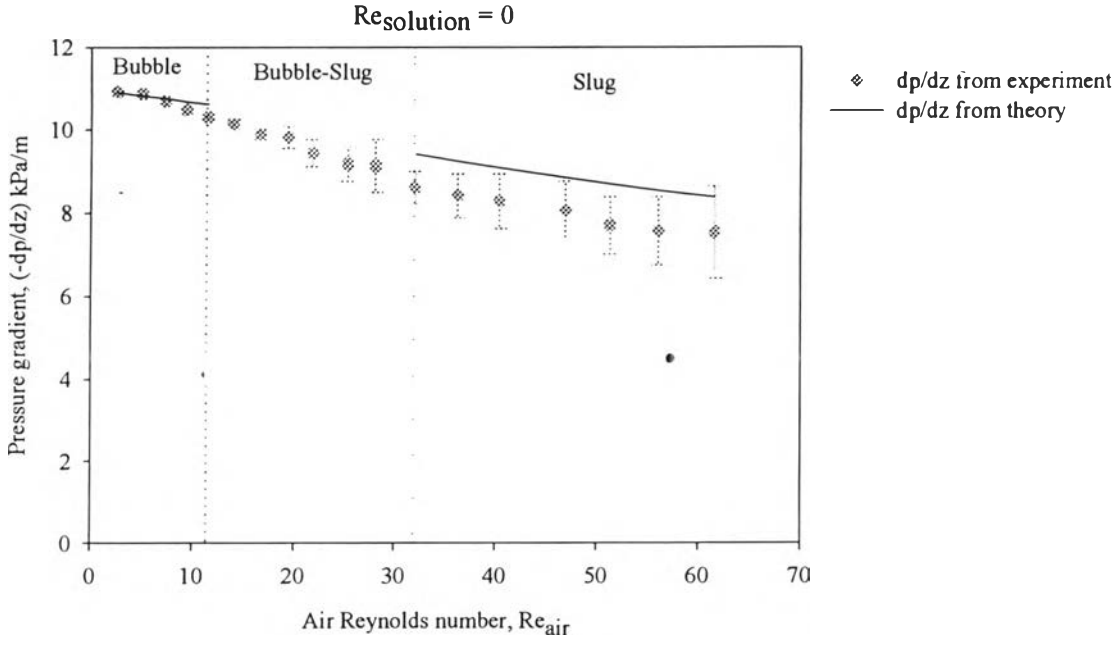

Figure 4.5 (b) Comparison between theory and experimental pressure gradient vs. air Reynolds number of 50 vol% glycerol solution.

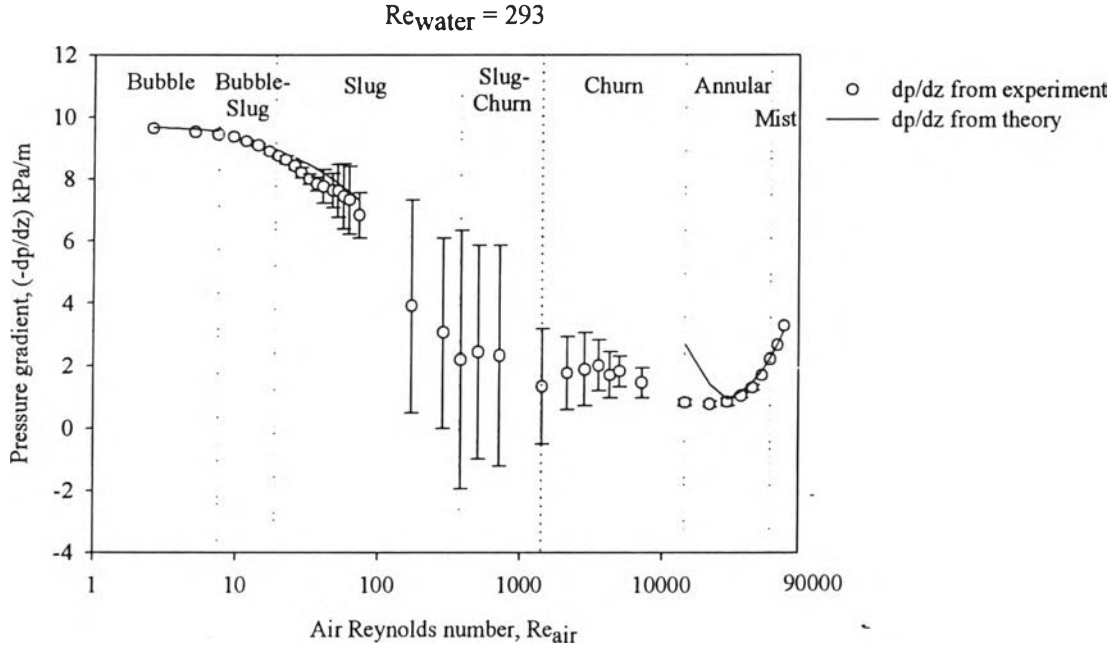

Figure 4.5 (c) Comparison between theory and experimental pressure gradient vs. air Reynolds number of pure water.

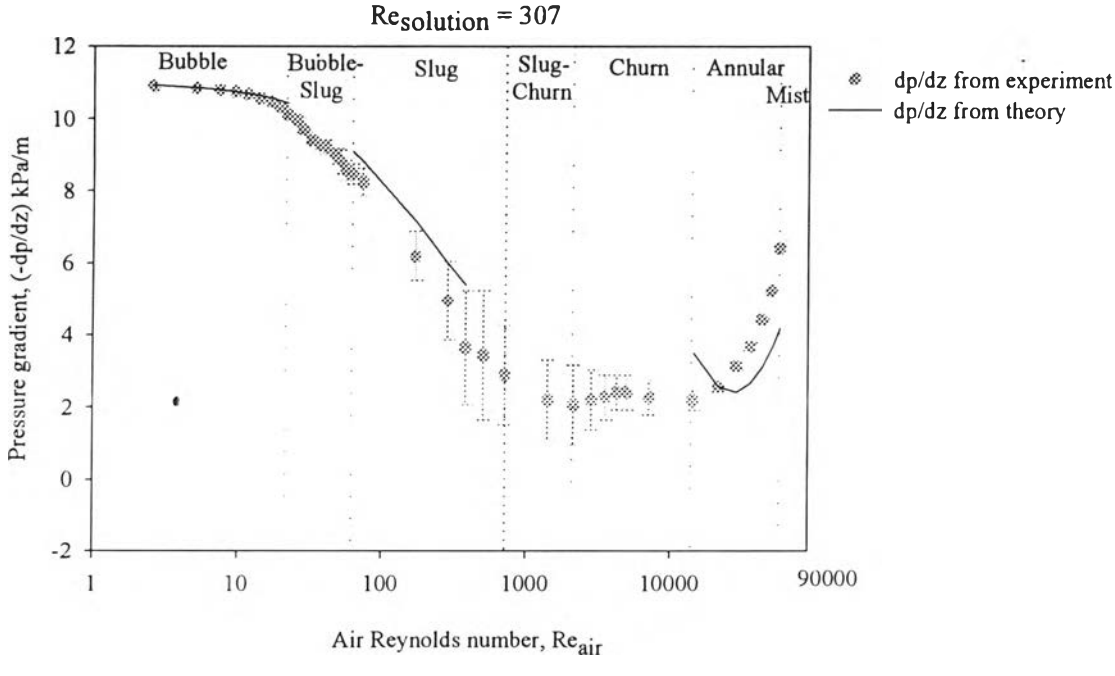

Figure 4.5 (d) Comparison between theory and experimental pressure gradient vs. air Reynolds number of 50 vol% glycerol solution.

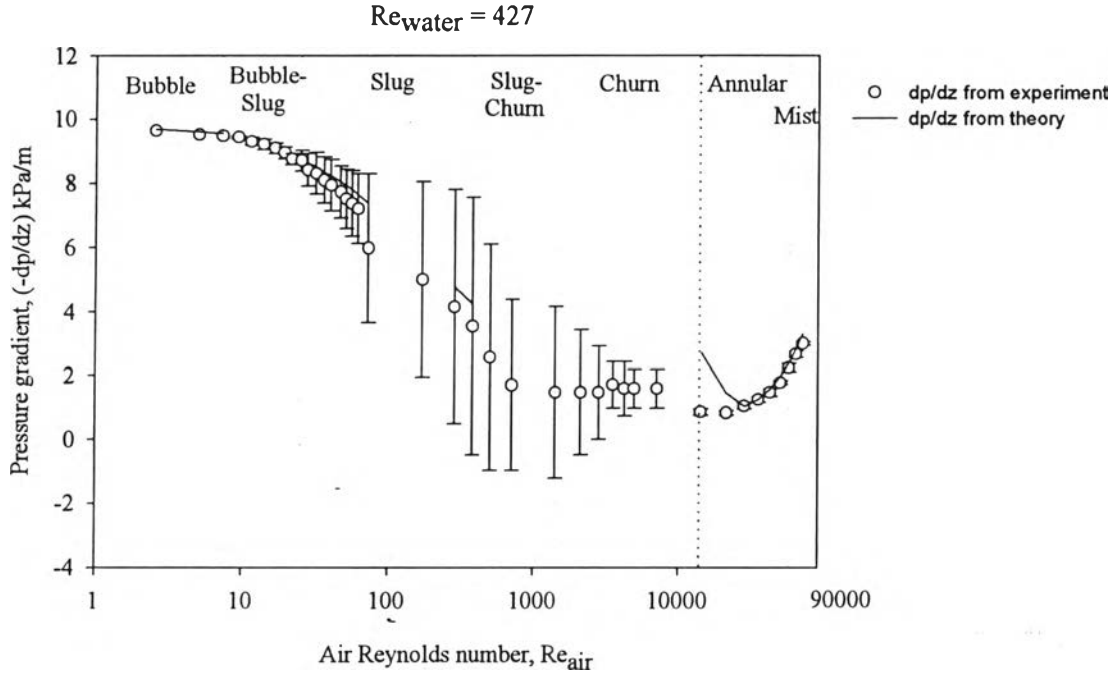

Figure 4.5 (e) Comparison between theory and experimental pressure gradient vs. air Reynolds number of pure water.

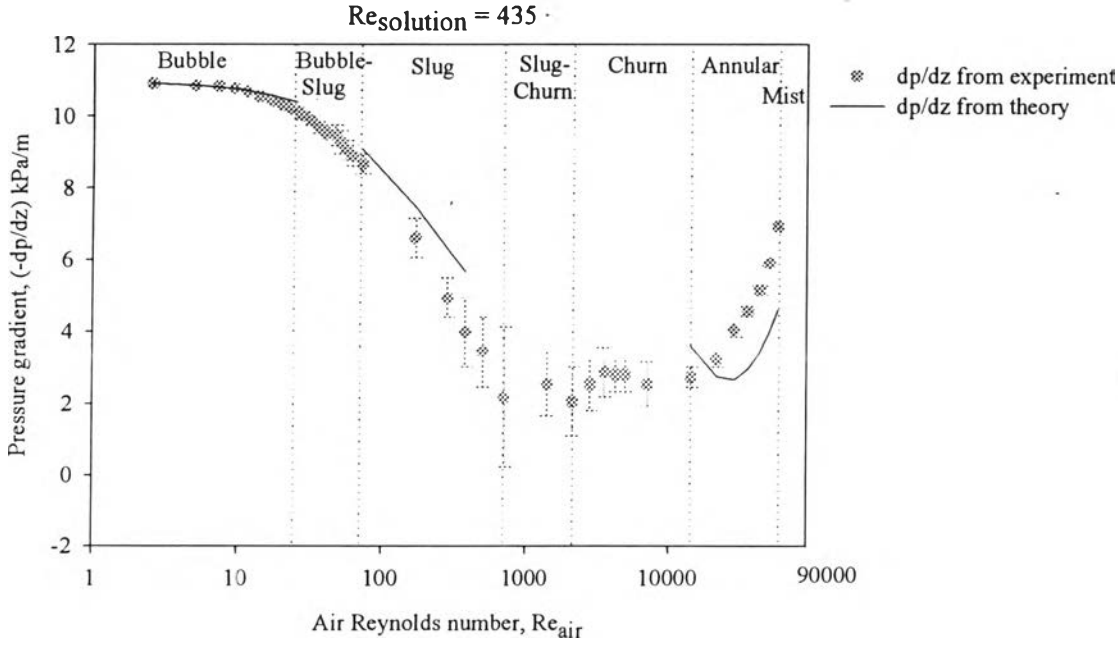

Figure 4.5 (f) Comparison between theory and experimental pressure gradient vs. air Reynolds number of 50 vol% glycerol solution.

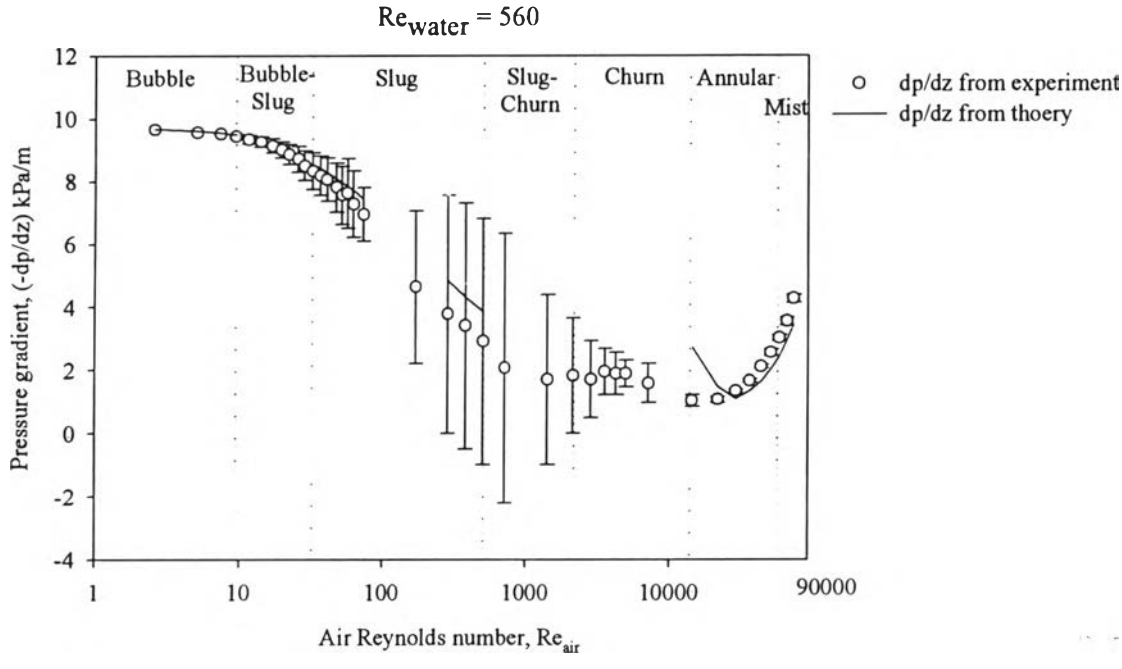

Figure 4.5 (g) Comparison between theory and experimental pressure gradient vs. air Reynolds number of pure water.

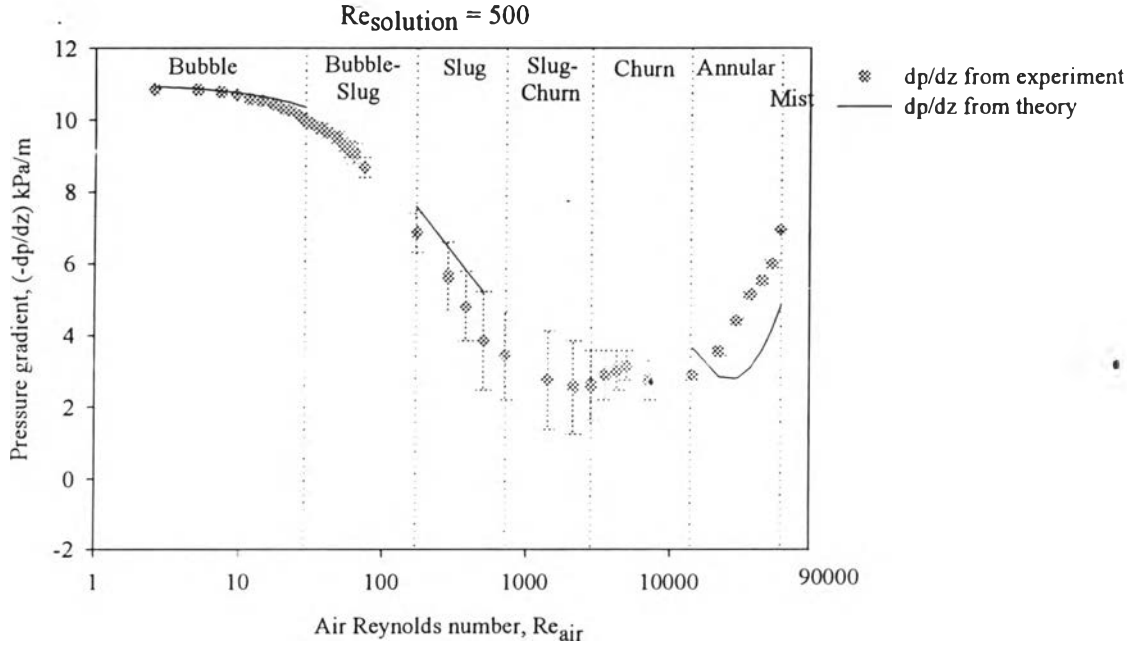

Figure 4.5 (h) Comparison between theory and experimental pressure gradient vs. air Reynolds number of 50 vol% glycerol solution.

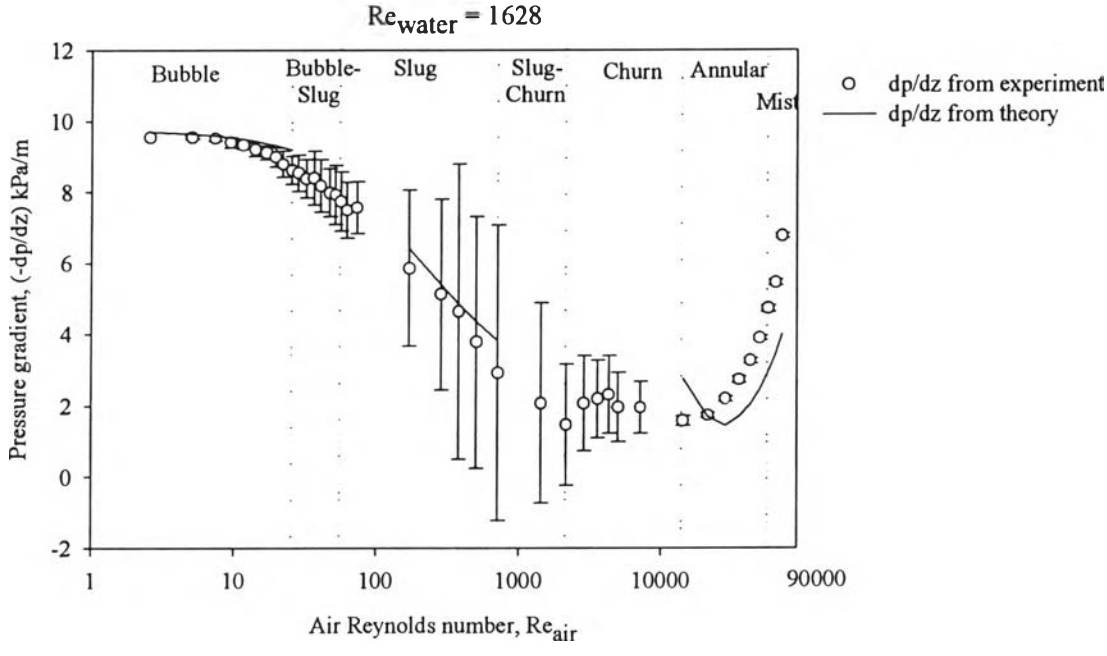

Figure 4.5 (i) Comparison between theory and experimental pressure gradient vs. air Reynolds number of pure water.

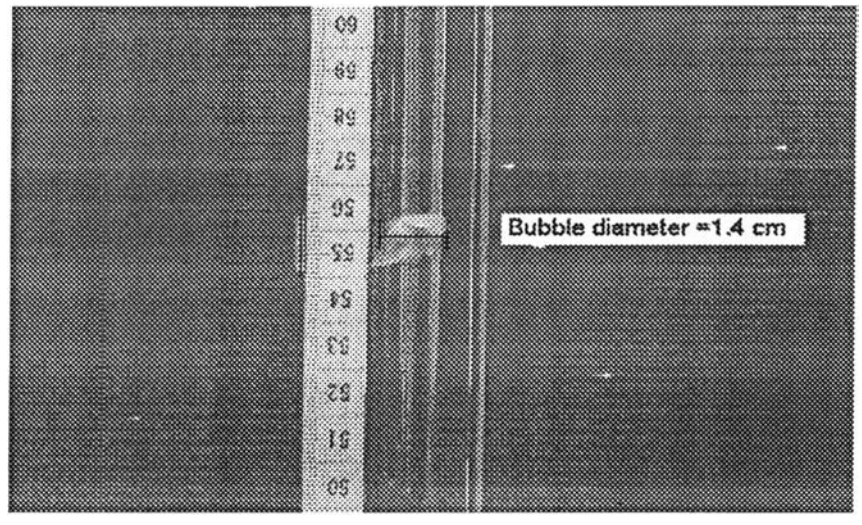

Figure 4.6 (a) Bubble size diameter in air-pure water mixture.

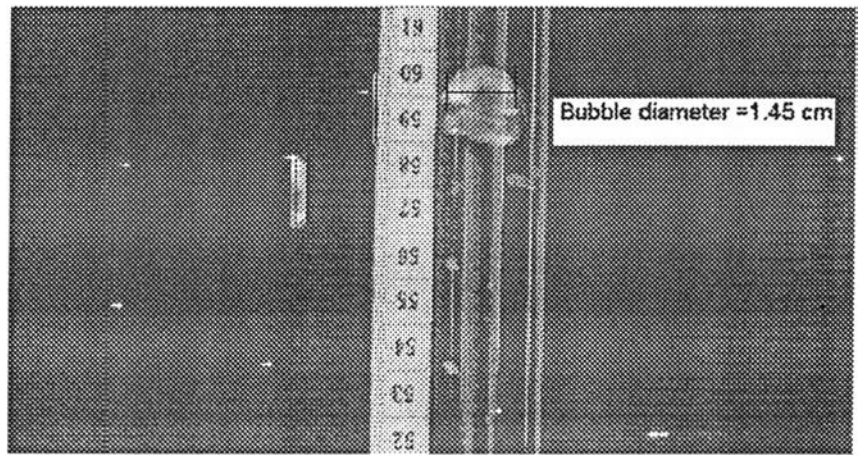

Figure 4.6 (b) Bubble size diameter in air-pure water mixture.

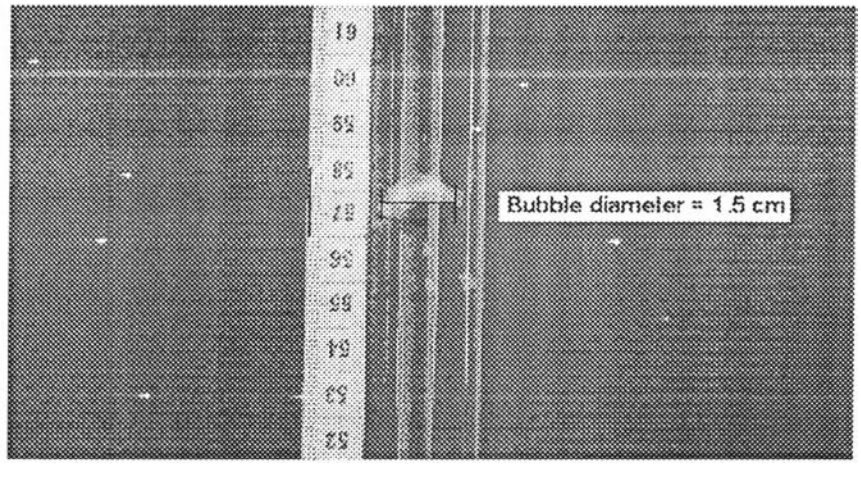

Figure 4.6 (c) Bubble size diameter in air-50 vol% glycerol solution mixture.

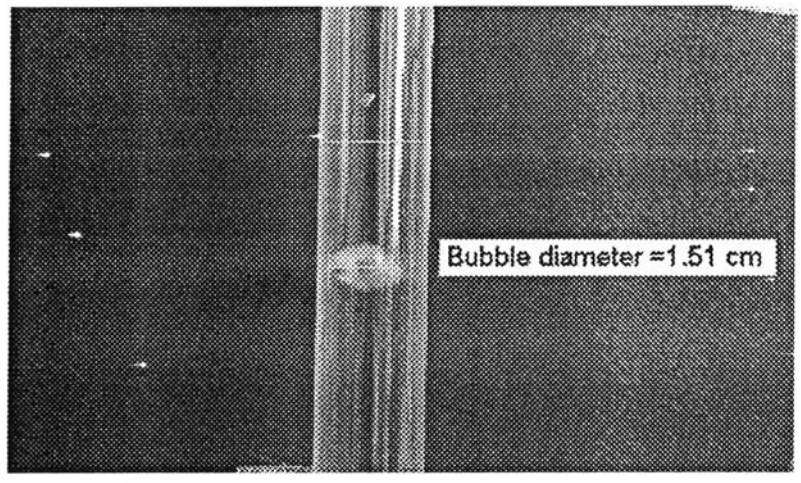

Figure 4.6 (d) Bubble size diameter in air-50 vol% glycerol solution mixture.

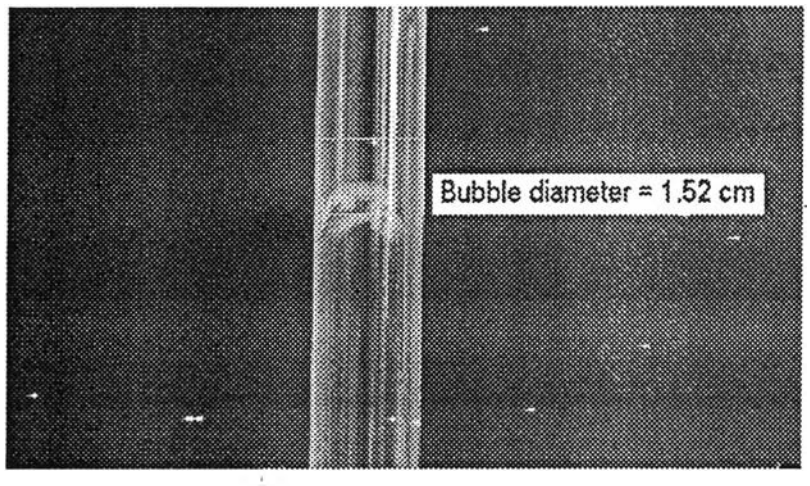

Figure 4.6 (e) Bubble size diameter in air-50 vol% glycerol solution mixture.

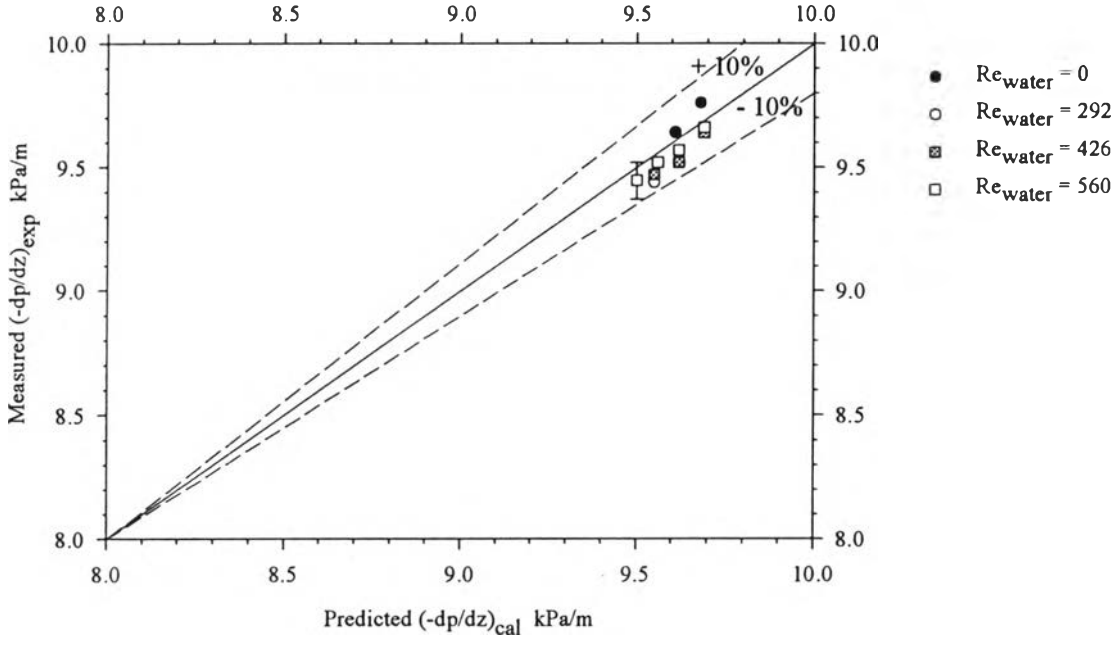

Figure 4.7 (a) Comparison between the theory and the measured pressure gradients for air-water mixture: bubble flow regime.

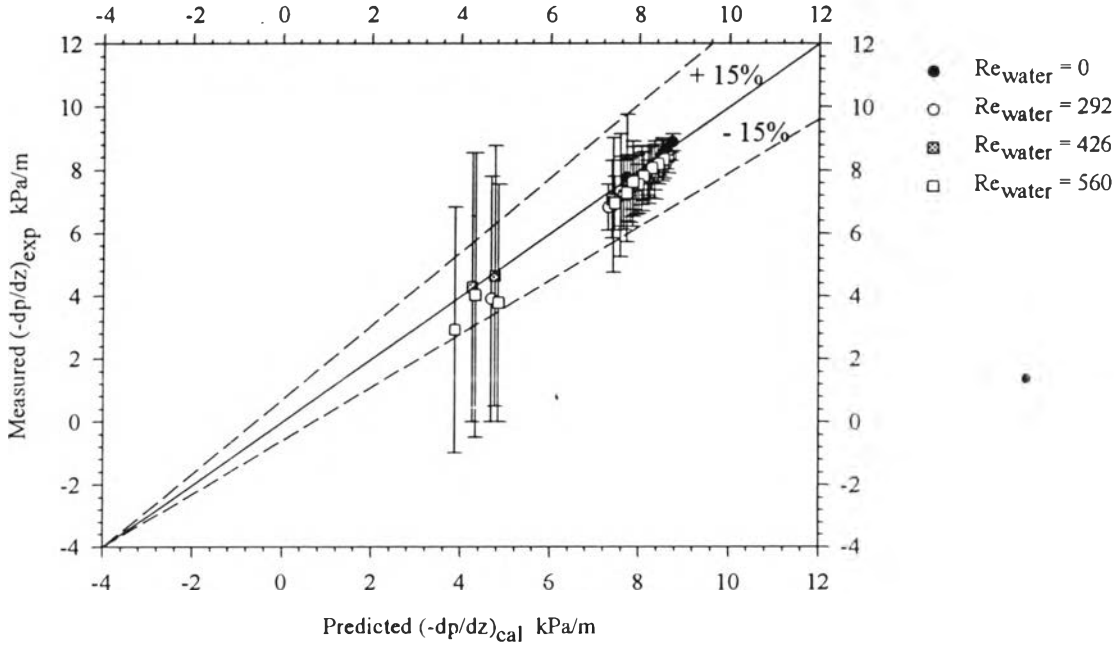

Figure 4.7 (b) Comparison between the theory and the measured pressure gradients for air-water mixture: slug flow regime.

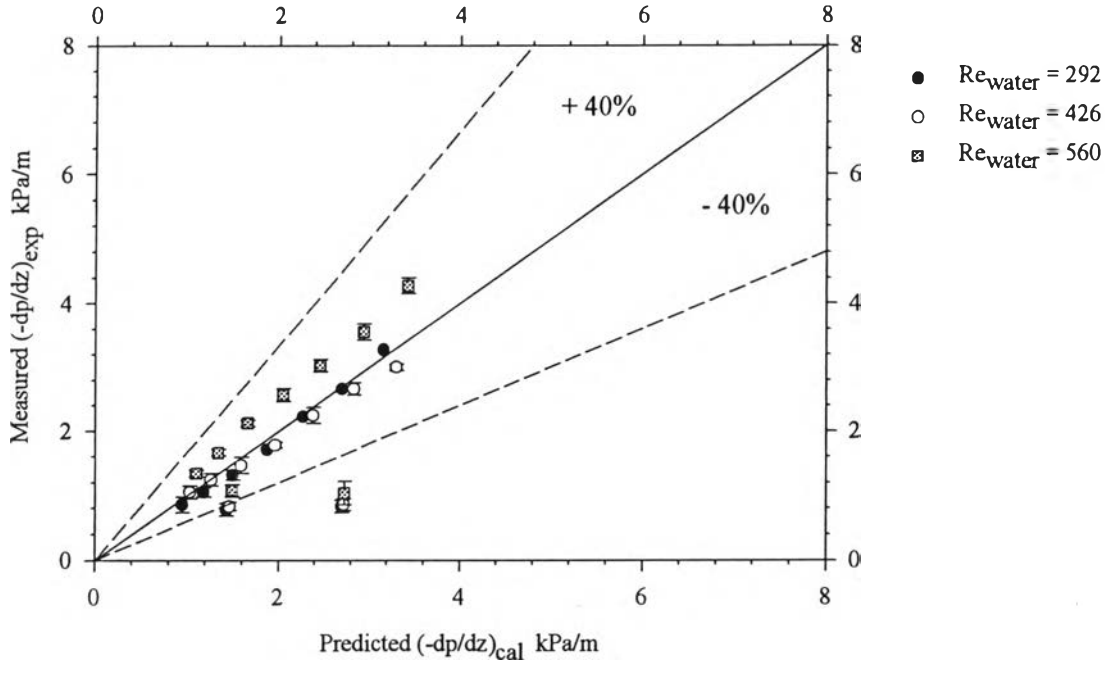

Figure 4.7 (c) Comparison between the theory and the measured pressure gradients for air-water mixture: annular and mist flow regime.

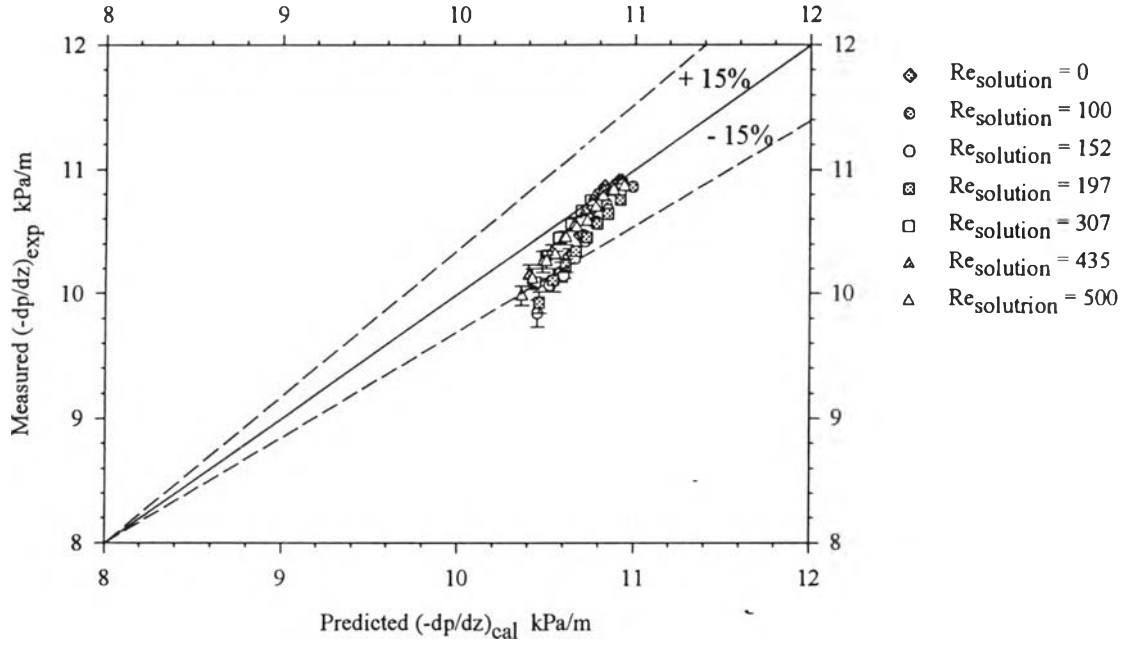

Figure 4.8 (a) Comparison between theory and experimental pressure gradients for the air-50 vol% glycerol solution mixture: bubble flow regime.

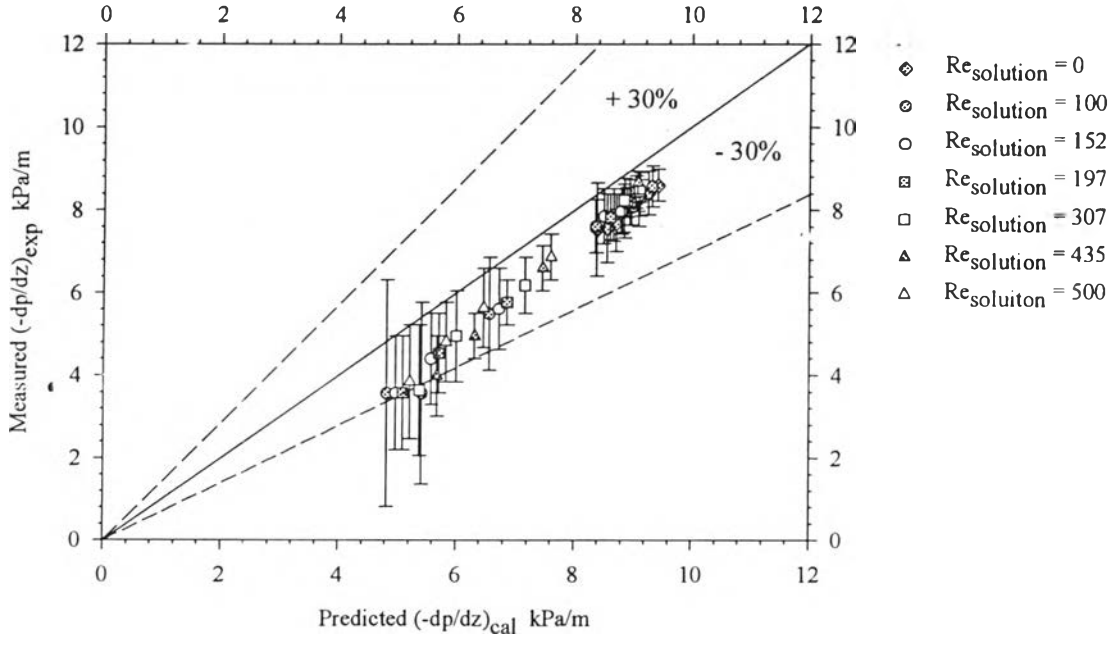

Figure 4.8 (b) Comparison between theory and experimental pressure gradients for the air-50 vol% glycerol solution mixture: Slug flow regime.

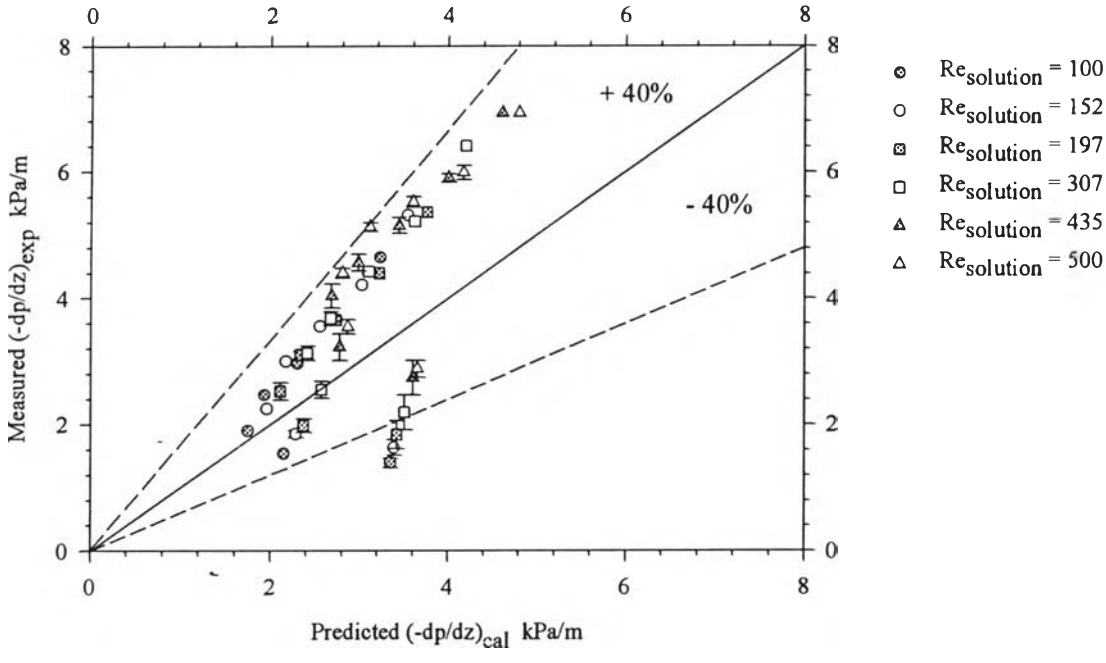

Figure 4.8 (c) Comparison between theory and experimental pressure gradients for the air-50 vol% glycerol solution mixture: annular and mist flow regime.